



柴北缘滩间山金矿黄铁矿微量元素特征： 指示多阶段金矿化事件

蔡鹏捷^{1,2}, 郑有业^{2,3}, 鲁立辉³, 陈 鑫³, 殷悦铭³, 侯维东³, 韩登辉³, 许荣科²

(1. 广州海洋地质调查局, 广州 510760;
2. 中国地质大学(武汉) 地质调查研究院, 武汉 430074;
3. 中国地质大学(武汉) 资源学院, 武汉 430074)

摘要: 滩间山金矿是位于我国柴达木北缘(柴北缘)中的典型的造山型金矿。本次工作利用激光剥蚀电感耦合等离子体质谱(LA-ICP-MS)对滩间山金矿主要载金黄铁矿进行微量元素分析; 通过野外实地调查及室内显微镜下观察, 将载金黄铁矿分为四类: 蚀变炭质糜棱片岩型黄铁矿(Py1)、石英脉型浸染状黄铁矿(Py2)、石英脉型团块状黄铁矿(Py3)、脉岩中浸染状黄铁矿(Py4)。结果表明, 黄铁矿 Py1 到 Py4 的微量元素特征指示其温度逐渐升高, 结合矿区同位素年代学资料, 认为不同类型黄铁矿对应滩间山金矿成矿演化过程四阶段中的后三阶段: 海西早期, 构造挤压 Au 矿化富集阶段(Py1); 海西晚期, 构造伸展阶段 Au 矿化叠加富集阶段(Py2, Py3); 印支期, 柴达木-祁连地体地壳抬升 Au 矿化再富集阶段(Py4)。

关键词: 滩间山; 造山型金矿; 黄铁矿; 微量元素; 成矿演化

文章编号: 1004-0609(2019)-10-2381-13

中图分类号:

文献标志码: A

黄铁矿广泛形成于沉积岩、岩浆岩和变质岩中, 不但是地壳中分布最广的硫化物, 而且是大多数金矿床中重要的载金矿物^[1-3]。黄铁矿通常含有重要的微量元素, 如 Cu、Ni、As、Co、Au、Ag、Pb、Zn、Sb、Se、Te、Hg、Tl 和 Bi 等, 这些元素特征具有重要的指示意义^[4-5]。通过测定黄铁矿微量元素的含量和比值, 可推断黄铁矿的类型与成因, 可提供成矿物质来源、成矿流体来源及矿床成因等信息^[6-9]。随着激光剥蚀电感耦合等离子体质谱仪(LA-ICP-MS)应用的发展, 学者们开始应用其对黄铁矿进行微区的微量元素分析^[10-17]。黄铁矿的微区分析能更好地反应微量元素在不同的黄铁矿类型中的差异, 从而指示成矿流体的复杂化学特征^[18], 包括热液系统的温度变化^[19]、成矿流体物质来源^[20]和氧化还原环境^[21], 甚至可用于反映古气候变化^[22]。因此, 对黄铁矿微量元素特征的研究, 有助于探讨矿床成因, 且对矿床的勘查及矿石的回收、综合利用都具有重要意义^[23]。黄铁矿微区微量元素研究仍处于起步阶段, 从目前所得到的一些重要的科研成果来看, 表明它为金矿成矿作用研究提供了一个新的途径^[1, 24-26], 但对于造山型金矿的黄铁矿微区微量

元素研究还相对较少。

滩间山金矿位于柴达木盆地北缘(以下简称“柴北缘”)中西段, 至今为止仍是柴北缘地区规模最大的金矿床, 金资源量达到 50.4 t^[27]。滩间山金矿经历了早古生代和晚古生代至早中生代的多次增生和碰撞造山运动, 前人研究认为滩间山金矿是两次碰撞造山运动的产物^[27-28]。本文针对滩间山金矿中不同含金岩石类型的载金黄铁矿进行 LA-ICP-MS 微量元素分析, 以期进一步揭示黄铁矿的成因和微量元素特征, 同时结合滩间山金矿成矿时代, 为滩间山金矿成矿演化过程的研究提供来自黄铁矿微量元素的证据。

1 地质背景

柴北缘地处柴达木板块与祁连板块的交接部位, 以产出柴北缘超高压变质带及其相关研究闻名于世^[29-35]。其东起青海省都兰县的野马滩, 西至阿尔金断裂带附近的小赛什腾山, 呈北西向绵延超过 900 km, 其南北边界分别为柴北缘深断裂和拉脊山-中祁

基金项目: 教育部长江学者和创新团队发展计划资助项目(IRT14R54); 中国地质调查局项目(21201011000150004, DD20190069)

收稿日期: 2018-08-26; 修订日期: 2019-01-21

通信作者: 许荣科, 副教授, 博士; 电话: 18971071732; E-mail: xurongke1968@126.com

连南缘断裂，东西则分别以哇洪山—温泉断裂和阿尔金走滑断裂为界^[29~35]，大型韧性剪切带和超高压变质带则形成于造山过程中^[29~35]。该地区经历了复杂构造演化，岩浆活动频繁，成矿地质条件优越，前人开展过一系列的找矿与基础地质工作^[36~43]。

滩间山金矿区位于柴北缘西段，主要出露中元古界万洞沟群炭质绢云片岩、钙质片岩、炭质千枚岩和炭质糜棱片岩、炭质大理岩和白云质大理岩，总体呈NW向展布，其中炭质千枚岩—糜棱片岩是主要的容矿地层^[27, 44]。矿区构造发育，发育有两组褶皱构造，NW向复式向斜和近SN向层间背向形。3组脆性断裂构造，分别为NW向、NNE向及近EW向断裂构造(见图1)。岩浆岩主要形成于华里西—印支期^[44]，以酸性岩(斜长花岗斑岩、花岗斑岩、花岗细晶岩、闪长玢岩)为主，及少量中性岩(云煌岩)，且大多呈小岩株或岩脉产出。矿区内地体主体为NNE向展布，少数呈NW向展布，矿体形态以层状、脉状为主，与蚀变围岩无明显界线，呈渐变过渡关系(见图2(a))。矿石类型主要为蚀变炭质千枚岩—片岩型和蚀变脉岩型。矿石矿物主要为自然金、银金矿、毒砂、黄铁矿等，脉石矿物主要为石英、绢云母、绿泥石、绿帘石、白云石等^[28]。

2 样品及黄铁矿类型划分

根据矿区野外地质考察及显微镜下矿物特征，滩间山金矿中含矿黄铁矿主要划分为以下四类：糜棱岩化含炭千枚岩中条带状黄铁矿(简称Py1)，顺千枚岩面理产出，从截面看成条带状(见图2(b))，均呈浅黄色，晶体形态为自形—半自形，粒状结构(见图2(f))，含量占全岩5%~10%；含炭千枚岩内石英脉中浸染状黄铁矿(简称Py2)，浅黄色，呈星散状分布于石英脉内(见图2(c))，晶体形态多为四方及六方晶形(见图2(g))，含量占石英脉1%~3%；石英脉中团块状黄铁矿(简称Py3)，呈团块状集合体形成于石英脉与含炭千枚岩接触位置(见图2(d))，晶体形态为自形—半自形，块状结构(见图2(h))，含量占石英脉20%~30%；蚀变花岗斑岩脉岩中黄铁矿(简称Py4)，呈浸染状分布(见图2(e))，四方—六方晶形，粒状结构(见图2(i))，含量占全岩5%~10%；根据黄铁矿寄主岩石的穿切关系及构造形态，从早到晚依次为Py1、Py2、Py3、Py4。

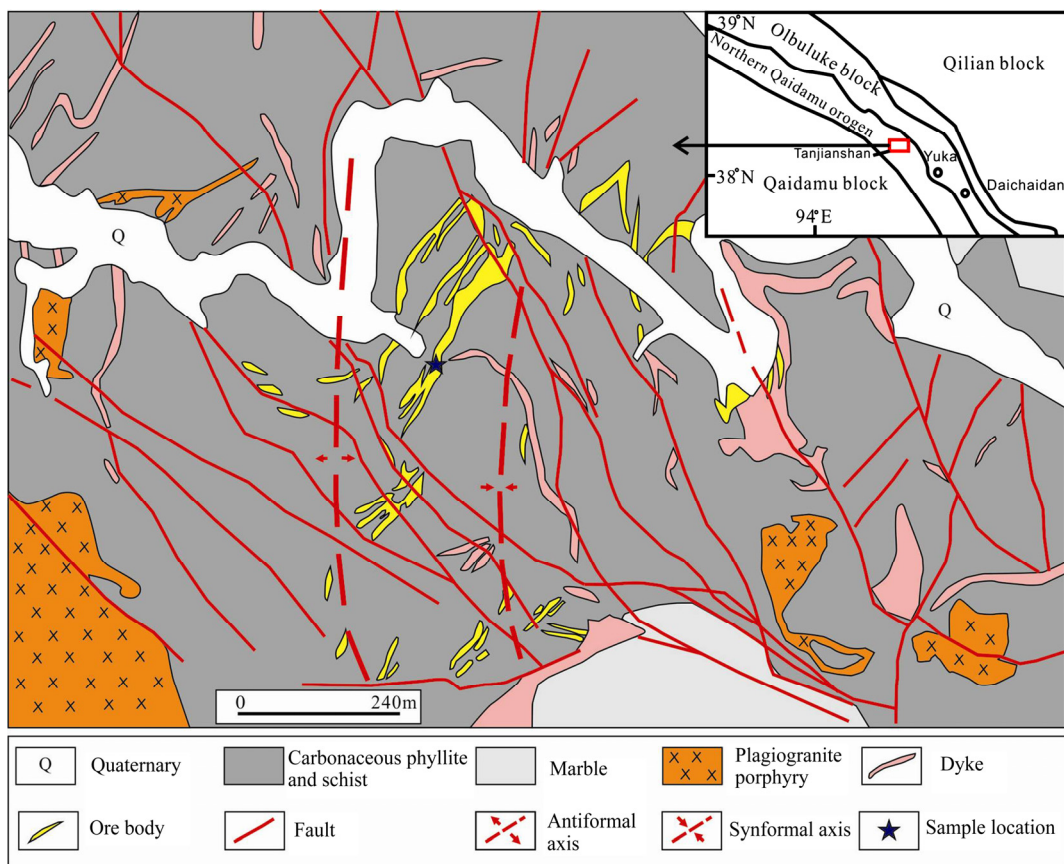


图1 滩间山金矿区地质略图(据文献[28])

Fig. 1 Geological sketch map of Tanjianshan gold deposit district (Derived from Ref. [28])

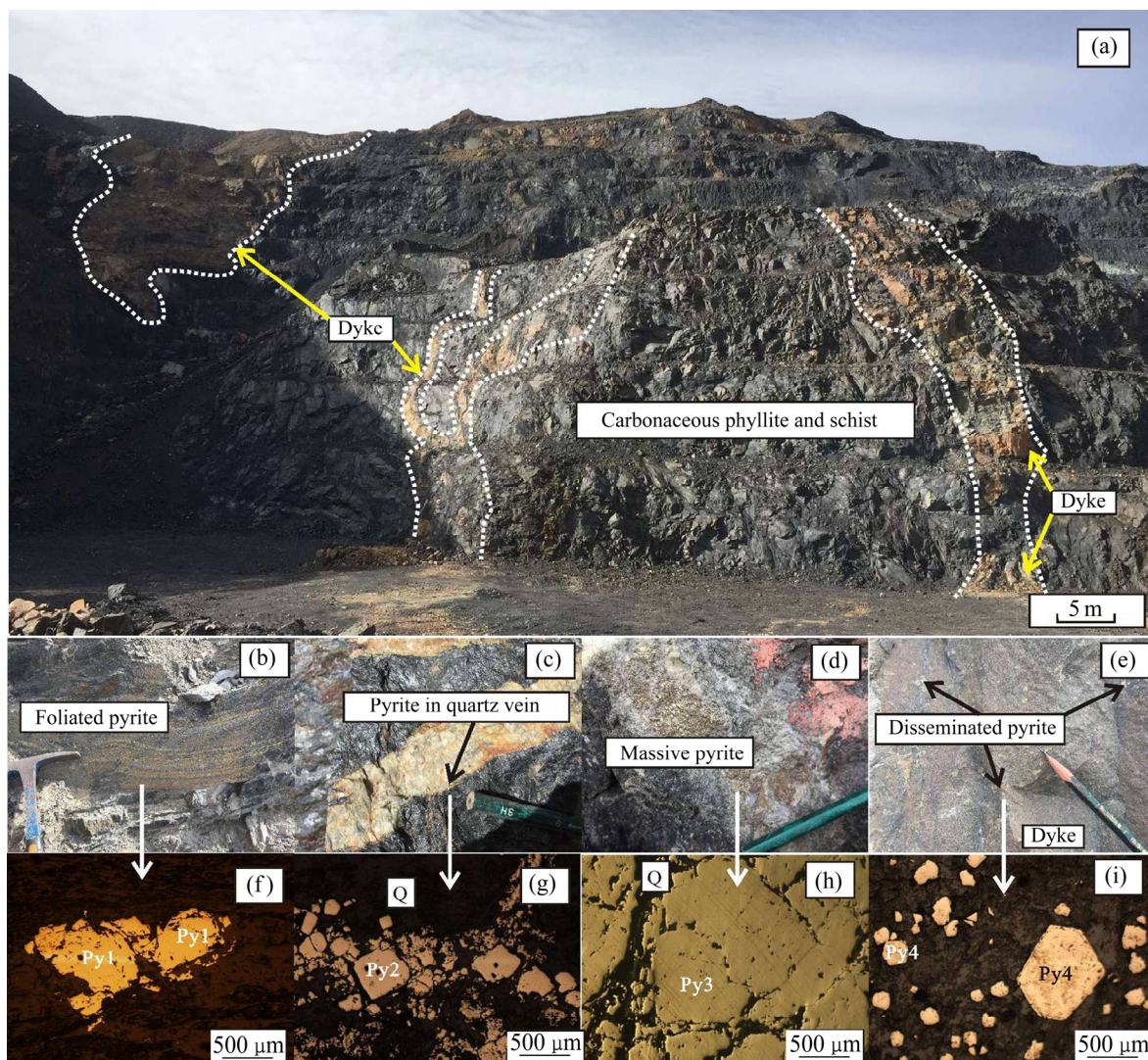


图2 滩间山金矿野外及镜下特征(Q—石英; Py—黄铁矿): (a) 金矿区野外照片; (b) 含炭千枚岩中条带状黄铁矿(Py1); (c) 含炭千枚岩内石英脉中浸染状黄铁矿(Py2); (d) 石英脉中团块状黄铁矿(Py3); (e) 蚀变花岗斑岩脉岩中浸染状黄铁矿(Py4); (f) 含炭千枚岩黄铁矿(Py1); (g) 石英脉中黄铁矿(Py2); (h) 团块状黄铁矿(Py3); (i) 脉岩中黄铁矿(Py4)

Fig. 2 Field photographs and photomicrographs of Tanjianshan gold deposit (Q—Quartz; Py—Pyrite): (a) Gold deposit field photographs; (b) Striped pyrite (Py1) in carbonaceous phyllite; (c) Disseminated pyrite (Py2) in quartz veins of carbonaceous phyllite; (d) Massive pyrite (Py3) in quartz vein; (e) Disseminated pyrite (Py4) in altered granite porphyry dyke; (f) Pyrite (Py1) in carbonaceous phyllite; (g) Pyrite (Py2) in quartz vein; (h) Disseminated pyrite (Py3); (i) Pyrite (Py4) in granite porphyry dyke

3 测试方法

本研究所采集的代表性样品分别被制成薄片和光片, 在显微镜下观察鉴定和标记后, 进行黄铁矿原位微区主微量元素含量分析。测试过程在武汉上谱分析科技有限责任公司利用 LA-ICP-MS 完成, 详细的仪器参数和分析流程见文献[45]。GeolasPro 激光剥蚀系统由 COMPexPro 102 ArF 193 nm 准分子激光器和 MicroLas 光学系统组成, ICP-MS 型号为 Agilent

7700e。激光剥蚀过程中采用氦气作载气、氩气为补偿气以调节灵敏度, 二者在进入 ICP 之前通过一个 T型接头混合, 激光剥蚀系统配置有信号平滑装置^[46]。本次分析的激光束斑和频率分别为 44 μm 和 5Hz。单矿物微量元素含量处理中, 采用玻璃标准物质 NIST 610、NIST 612 进行多外标无内标校正^[46], USGS 的硫化物标准物质 MASS-1 作为监控标样验证校正方法的可靠性。每个时间分辨分析数据包括 20~30 s 空白信号和 50 s 样品信号。对分析数据的离线处理(包括对样品和空白信号的选择、仪器灵敏度漂移校正以及元素含量计算)采用软件 ICPMSDataCal^[47]完成。

示,四种类型黄铁矿在微量元素组成上存在较大差异。

Py1 黄铁矿相对贫 Ti(平均值为 3.60×10^{-6})、Cr(平均值为 0.90×10^{-6})、Cu(平均值为 0.49×10^{-6})、Co(平均值为 41.79×10^{-6})、As(平均值为 190.46×10^{-6})、Ag(平均值为 0.10×10^{-6})、Au(平均值为 0.01×10^{-6})、

4 分析结果

本次滩间山含金黄铁矿微量元素组成如表 1 所

表 1 滩间山金矿黄铁矿 LA-ICP-MS 微量元素分析结果($\times 10^{-6}$)

Table 1 Trace element analysis for pyrite from Tanjianshan gold deposit determined by LA-ICP-MS ($\times 10^{-6}$)

Pyrite type	Sample No.	Ti	Cr	Mn	Cu	Co	Ni	Zn	As	Se	Sn	Pb	Bi	Ag	Cd	Sb	Au
Py1	TJS-1-01	3.87	4.32	0.50	1.05	22.0	197	0.10	309	0.96	0.27	8.76	2.51	0.13	—	0.72	0.01
	TJS-1-02	3.74	1.53	—	0.07	42.1	249	0.17	35.5	4.28	0.17	0.61	0.09	—	0.07	0.04	0.02
	TJS-1-03	3.61	—	0.90	0.67	36.4	215	—	300	9.67	—	11.5	3.24	0.17	0.05	0.92	0.02
	TJS-1-04	3.02	0.12	—	0.00	63.2	311	—	45.4	—	0.26	1.04	0.29	0.02	—	0.04	0.01
	TJS-1-05	4.15	1.43	1.13	1.32	27.6	236	1.33	394	8.34	—	19.7	5.70	0.20	0.04	0.84	0.01
	TJS-1-06	3.98	0.26	—	0.00	69.5	326	—	64.6	—	0.35	1.16	0.46	0.03	—	0.07	0.01
	TJS-1-07	3.57	—	0.66	0.72	23.4	227	—	283	3.74	0.19	10.9	3.12	0.17	—	0.88	0.02
	TJS-1-08	2.68	—	—	0.00	53.0	290	—	41.3	0.60	0.12	0.95	0.21	0.01	—	0.04	0.01
	TJS-1-09	3.84	1.27	0.80	0.99	17.3	220	0.70	347	2.99	0.04	13.8	4.03	0.16	0.02	0.80	0.01
	TJS-1-10	3.55	0.08	—	0.05	63.5	290	—	83.9	—	0.19	1.62	0.56	0.03	0.00	0.06	0.01
Py2	TJS-2-1	3.24	0.83	14.5	12.2	113	341	1.78	1444	0.97	—	45.3	0.39	0.78	—	85.5	0.16
	TJS-2-2	3.12	0.72	13.7	11.0	107	319	1.81	1315	0.85	—	39.6	0.30	0.80	—	77.2	0.13
	TJS-2-3	3.59	0.82	14.2	13.4	114	361	1.85	1521	1.88	—	46.1	0.61	0.86	—	86.8	0.14
	TJS-2-4	5.38	—	0.03	0.49	254	520	0.30	240	117	0.38	0.15	0.50	0.01	—	0.11	0.13
	TJS-2-5	3.98	0.96	13.3	12.0	112	378	1.69	1545	1.98	—	41.8	0.54	0.83	—	79.8	0.10
	TJS-2-6	5.34	—	—	0.45	212	539	0.31	222	128	0.26	0.16	0.45	—	—	0.11	0.14
	TJS-2-7	3.75	5.90	0.55	90.7	48.5	313	4.15	8568	8.36	0.34	30.0	0.68	0.67	0.17	23.5	0.18
	TJS-2-8	4.12	2.68	0.30	103	47.1	337	5.58	10199	5.67	0.40	34.0	0.74	0.72	0.14	25.8	0.21
	TJS-2-9	3.62	2.97	—	108	45.1	319	0.85	10548	7.20	0.58	29.4	0.65	0.56	0.09	21.4	0.19
	TJS-2-10	4.34	0.81	0.19	80.8	39.6	322	8.75	8519	8.39	0.19	37.3	0.75	0.83	0.23	30.1	0.19
Py3	TJS-3-1	412	2.74	3.39	139	46.7	125	—	23832	—	0.26	132	1.92	4.64	0.10	39.07	4.40
	TJS-3-2	8581	13.2	9.43	153	367	534	3.22	11198	—	0.85	561	17.6	14.8	0.06	194	1.47
	TJS-3-3	635	0.60	1.64	109	87.6	148	—	27629	—	0.40	129	3.29	3.88	—	37.7	1.48
	TJS-3-4	9227	10.3	9.05	142	335	459	2.99	12778	—	0.81	478	14.8	13.0	0.06	171	1.28
	TJS-3-5	459	5.33	—	88	68.0	58.0	0.13	28121	6.88	0.16	65.0	0.23	1.24	—	25.7	1.52
	TJS-3-6	561	0.61	2.16	120	86.1	148	—	26538	—	0.29	127	3.10	3.64	0.04	37.8	1.30
	TJS-3-7	8376	17.9	8.43	129	312	396	2.82	16252	—	0.66	397	12.4	11.0	0.05	143	1.10
	TJS-3-8	597	0.75	3.37	120	61.8	127	—	26629	—	0.14	122	2.62	4.24	0.13	39.1	3.83
	TJS-3-9	8928	11.8	9.29	152	360	518	3.19	11347	—	0.86	547	17.1	14.6	0.06	190	1.43
	TJS-3-10	459	0.56	2.76	119	66.4	127	—	24903	—	0.23	122	2.46	3.74	0.08	36.4	2.66
Py4	TJS-4-1	3.69	0.25	0.54	0.13	27.4	5.25	5.43	3485	—	0.19	0.03	—	—	0.06	—	0.03
	TJS-4-2	2.71	4.16	1.71	8.71	14.9	4.33	0.10	400	9.33	—	6.05	0.01	1.27	0.09	2.76	0.02
	TJS-4-3	3.07	0.87	0.06	1.60	41.0	13.0	—	36.2	—	0.78	0.11	0.01	0.04	0.07	—	0.02
	TJS-4-4	3.26	—	0.21	0.24	43.2	4.77	0.83	4042	—	0.48	0.01	—	0.02	—	—	0.05
	TJS-4-5	2.88	0.37	1.17	0.88	12.1	2.20	—	316	4.30	0.01	1.24	—	0.02	0.08	0.21	0.05
	TJS-4-6	3.73	—	—	0.24	45.7	5.94	0.77	4506	—	0.55	0.01	—	—	—	—	0.04
	TJS-4-7	2.73	0.10	0.97	1.18	11.4	2.78	—	278	2.63	—	1.24	0.01	—	0.06	0.17	0.05
	TJS-4-8	3.78	—	0.68	0.12	40.6	5.54	8.03	4324	—	0.51	0.01	—	0.06	—	0.02	0.05
	TJS-4-9	3.80	—	—	0.19	35.1	5.29	4.00	4096	—	0.39	0.02	—	—	0.02	—	0.03
	TJS-4-10	2.69	9.60	1.07	7.15	11.7	3.86	0.19	310	2.94	—	10.6	0.02	1.00	0.05	2.11	0.04

Bi(平均值为 2.02×10^{-6})、Pb(平均值为 7.01×10^{-6})、富Ni(平均值为 256.14×10^{-6})。

Py2 黄铁矿相对于 Py1 黄铁矿具有近似的 Ti(平均值为 4.05×10^{-6})、Cr(平均值为 1.57×10^{-6})、Bi(平均值为 0.56×10^{-6})含量、相对高的 Cu(平均值为 43.23×10^{-6})、Co(平均值为 109.14×10^{-6})、Ag(平均值为 0.61×10^{-6})、Au(平均值为 0.16×10^{-6})，较为富集 As(平均值为 4412.14×10^{-6})、Pb(平均值为 30.38×10^{-6})和 Ni(平均值为 375.09×10^{-6})。

Py3 黄铁矿的 Ni(平均值为 264.14×10^{-6})与 Py2、Py3 相当, 其中 Ti(平均值为 3823.43×10^{-6})、Cu(平均值为 127.09×10^{-6})、Co(平均值为 179.04×10^{-6})、Ag(平均值为 7.47×10^{-6})、Au(平均值为 2.05×10^{-6})、As(平均值为 20922.70×10^{-6})、Pb(平均值为 267.93×10^{-6})、Cr(平均值为 6.37×10^{-6})、Bi(平均值为 7.55×10^{-6})等微量元素含量均高于其他三类黄铁矿的。

Py4 黄铁矿的 Ni(平均值为 5.29×10^{-6})含量低于其他三类黄铁矿, 相对低 Cu(平均值为 2.04×10^{-6})、Bi(平均值为 0.01×10^{-6}), 其中 Ti(平均值为 3.23×10^{-6})、Cr(平均值为 1.92×10^{-6})、Co(平均值为 28.30×10^{-6})、As(平均值为 2179.27×10^{-6})、Ag(平均值为 0.40×10^{-6})、Au(平均值为 0.04×10^{-6})、Pb(平均值为 1.94×10^{-6})等微量元素含量低于 Py3 黄铁矿的, 近似于 Py2 黄铁矿的。

5 讨论

5.1 成矿温度

张德全等^[27, 37]在滩间山金矿中主要发现两类含矿石英脉, 第一类石英脉(Qz1)仅在 NW 向剪切带内的炭质糜棱岩片岩中观察到, 它与早期形成的黄铁矿(Py1)一起作为旋转的椭圆形斑状碎屑出露(见图 2(b))。第二类是与 Py 2 和 Py3 有关的细粒热液石英脉或黄铁矿石英细脉(Qz2)出现, 并广泛分布于受改造的炭质糜棱岩片岩和岩脉中(见图 2(c)~(d))。Qz1 的流体包裹体数据显示成矿流体具中-低温($186\sim250^{\circ}\text{C}$)和低盐度($1.4\%\sim7.9\% \text{ NaCl}_{\text{eqv}}$)的特点, 流体成分为 $\text{H}_2\text{O}-\text{CO}_2-\text{CH}_4-\text{NaCl}$ ^[27]。Qz2 含矿石英脉的流体包裹体则记录了两期热液和矿化事件, 一期盐度为 $1.8\%\sim7.9\% \text{ NaCl}_{\text{eqv}}$, 流体成分为 $\text{H}_2\text{O}-\text{CO}_2-\text{NaCl}$, 均一温度为 $274\sim289^{\circ}\text{C}$; 另一期盐度为 $1.6\%\sim10.8\% \text{ NaCl}_{\text{eqv}}$, 流体成分为 $\text{H}_2\text{O}-\text{NaCl}$, 均一温度为 $381\sim437^{\circ}\text{C}$ ^[27]。

一般认为黄铁矿内 Co/Ni 比值(即 $w(\text{Co})/w(\text{Ni})$)受到温度影响, Co/Ni 比值越大指示黄铁矿的形成温度越高^[48-51]。滩间山金矿内不同类型的黄铁矿 Co/Ni 比值如图所示(见图 3), Py1 的 Co/Ni 比值为 $0.10\sim1.16$ (平均值为 0.33), Py2 的 Co/Ni 比值为 $0.12\sim1.45$ (平均值为 0.46), Py3 的 Co/Ni 比值为 $0.37\sim1.18$ (平均值为 0.66), 表现出从 Py1 到 Py3 的 Co/Ni 比值逐渐升高, 指示黄铁矿的形成温度由低到高, 这与前人所观察到的炭质糜棱岩片岩中石英(Qz1)及后期侵入的石英脉(Qz2)中流体包裹体温度的三阶段温度变化是一致的。Py4 的 Co/Ni 比值($3.02\sim9.06$, 平均值为 5.52)是这几类黄铁矿中最高的, 指示其形成温度最高, 这与其形成于蚀变花岗斑岩脉岩有关。因此, 滩间山金矿中不同类型黄铁矿记录了多期金矿化的事件。

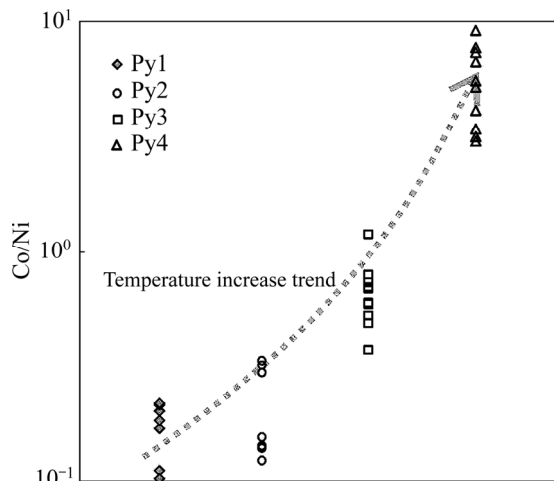


图 3 滩间山金矿不同类型黄铁矿 Co/Ni 比值

Fig. 3 Ratio of Co/Ni of different types of pyrite from Tanjianshan gold deposit

5.2 黄铁矿微量元素特征

黄铁矿中 Co、Ni 含量常常被用于指示其形成环境, 这是因其 Co 和 Ni 含量易受到黄铁矿沉淀时的物理化学条件影响^[3, 50]。在黄铁矿的 Co-Ni 成因图解中(见图 4), 表明 Py1、Py2、Py3 样品点大部分落在沉积改造区, 而 Py4 样品点主要落在岩浆区, 这与前面流体包裹体数据和 Co/Ni 比值指示的成矿温度变化是一致的。

从黄铁矿元素的相关性图解(见图 5)中可以看出: 在 Py1、Py2、Py3 中, Au、Ag、Cu、As、Pb、Bi 等元素的含量随 Co/Ni 比值升高而升高, 而在 Py4 中 Ag、Cu、As、Pb、Bi 等元素的含量则随 Co/Ni 比值升高而降低, 虽然 Py4 中 Au 和 As 元素的含量也随 Co/Ni

比值升高而升高,但与Py1、Py2、Py3并没有线性关系。故Py1、Py2、Py3与Py4的来源应该不同,Py1、Py2、Py3应该来自沉积地层,而Py4则来源于晚期岩浆。

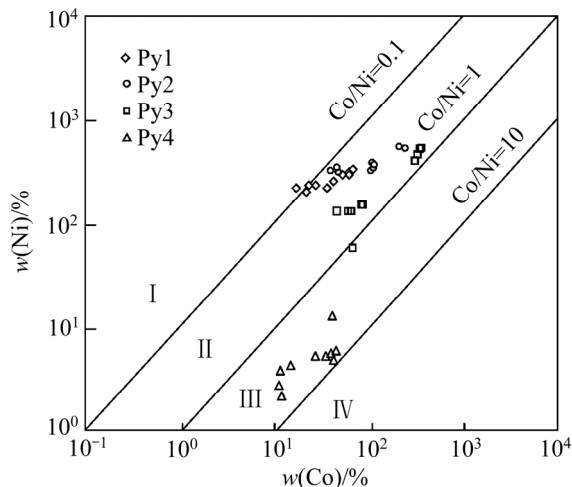


图4 滩间山金矿黄铁矿Ni-Co成因图解(底图据文献[51]):
I—沉积区; II—沉积改造区; III—岩浆区; IV—热液区

Fig. 4 Correlation of Co and Ni in pyrite from Tanjianshan gold deposit (Derived from Ref. [51]): I—Sedimentary field; II—Sedimentary reformation field; III—Magma field; IV—Hydrothermal field

5.3 成矿时代浅析

前人对柴周缘构造带中的金矿成矿时代进行了厘定:青龙沟金矿成矿时代为(409.4 ± 2.3) Ma(绢云母Ar-Ar法^[36]);赛坝沟金矿成矿时代为(425.5 ± 2.1) Ma(绢云母Ar-Ar法^[36])(426 ± 2) Ma(绢云母Ar-Ar法^[52]);野骆驼泉金矿成矿时代为(246.0 ± 3.0) Ma(绢云母Ar-Ar法^[36]);五龙沟金矿成矿时代为(236.5 ± 0.5) Ma(绢云母Ar-Ar法^[36]),(242.72 ± 1.69) Ma(黑云母Ar-Ar法^[53]);瑙木浑金矿成矿时代(227.8 ± 1.1) Ma(绢云母Ar-Ar法^[54]);大厂金矿成矿时代为(218.6 ± 3.2) Ma(绢云母Ar-Ar法^[36])。上述成矿时代指示了柴周缘构造带中的金矿大多与复合造山过程有关。

滩间山金矿区与成矿相关的年代学结果如图6和表2所示,也指示了滩间山金矿是一个与复合造山过程有关的金矿。将矿区黄铁矿微量元素变化、热事件时代和区域大地构造背景相结合可以推测,滩间山金矿的形成经历了至少四个阶段(见图7)。

第一阶段:中元古界裂谷期碎屑沉积物中Au的初步富集阶段(见图7(a))。伴随着裂谷的形成,形成半封闭—封闭的沉积环境,大量碎屑沉积物在此沉积。同时含Au热水顺深大断裂上升,与碎屑物发生沉积

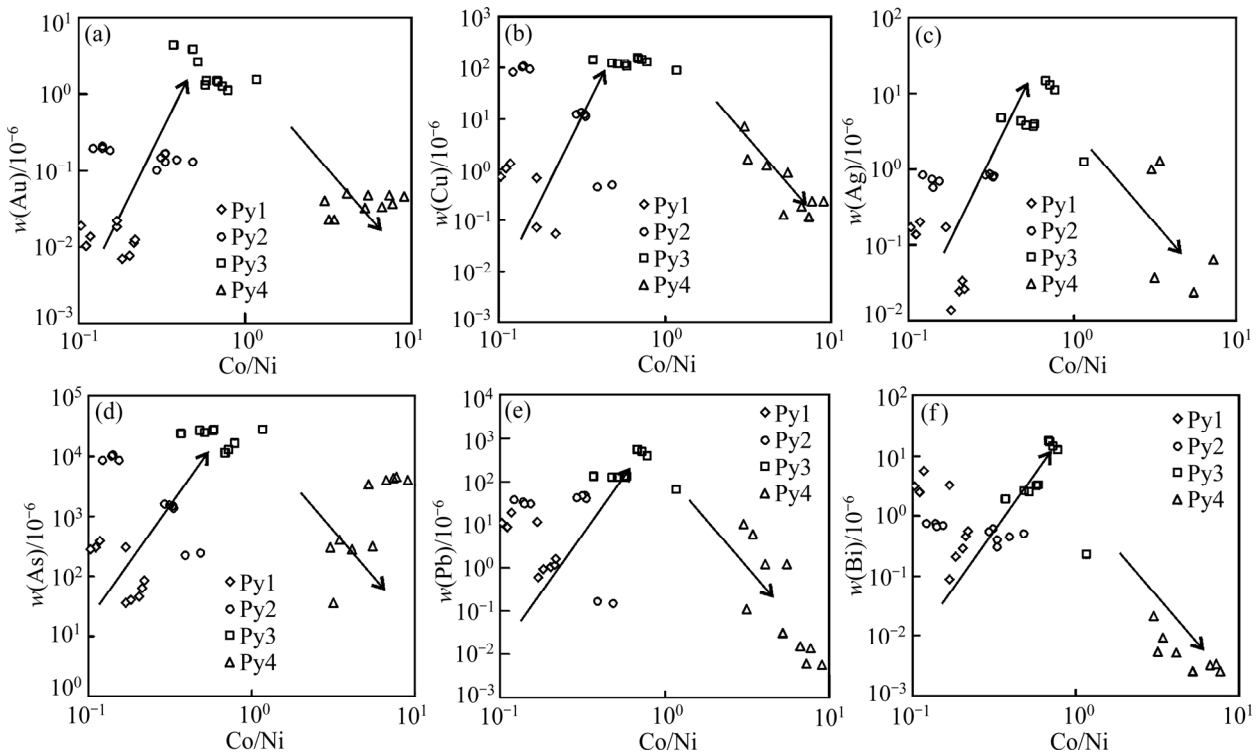


图5 滩间山金矿黄铁矿的部分微量元素相关性图解

Fig. 5 Correlation of selected trace elements in pyrite from Tanjianshan gold deposit: (a) Au—Co/Ni; (b) Cu—Co/Ni; (c) Ag—Co/Ni; (d) As—Co/Ni; (e) Pb—Co/Ni; (f) Bi—Co/Ni

表2 滩间山金矿区年龄数据

Table 2 Age data from Tanjianshan gold deposit

Sample type	Test method	Age/Ma	Data sources
Sericitization gold ore	Ar-Ar	409.4	Ref. [55]
Biotite in shear band	Ar-Ar	401	Ref. [36]
Plagioclase granite porphyry	Zircon U-Pb	394±6	Ref. [56]
Carbonaceous schist	K-Ar	385.8	Ref. [28]
Granite porphyry	Zircon U-Pb	356±2.8	Ref. [57]
Plagioclase granite porphyry	Zircon U-Pb	350.4±3.2	Ref. [41]
Granite porphyry	Zircon U-Pb	344.7±2	Ref. [58]
Mineralized altered granitoids (dike)	Zircon U-Pb	344±2.2	Ref. [56]
Trondhjemite porphyry	Rb-Sr	330±24.3	Ref. [55]
Plagiogranite porphyry (dyke)	K-Ar	309±4.77	Ref. [55]
Anorthosite aplite	K-Ar	309±4.8	Ref. [59]
Plagioclase granodiorite (dyke)	K-Ar	308.8±5.4	Ref. [28]
Pyritized sericite diorite porphyrite	K-Ar	294.29±4.39	Ref. [28]
Minette(dyke)	K-Ar	288.9±7.3	Ref. [28]
Diorite porphyrite (dyke)	K-Ar	289.6±6	Ref. [28]
Metamorphic veins	Rb-Sr	288	Ref. [27]
Sericite in fracture zone	Ar-Ar	284.04±2.95	Ref. [36]
Sericite in fracture zone	Ar-Ar	284	Ref. [36]
Granite porphyry (dyke)	K-Ar	275.9±7.2	Ref. [28]
Quartz diorite porphyrite	K-Ar	274.6	Ref. [60]
Altered granite porphyry (dyke)	K-Ar	268.94±4.31	Ref. [28]
Hydrothermal mineral	Ar-Ar	268.9	Ref. [27]
Plagiogranite porphyry (dyke)	K-Ar	209	Ref. [59]

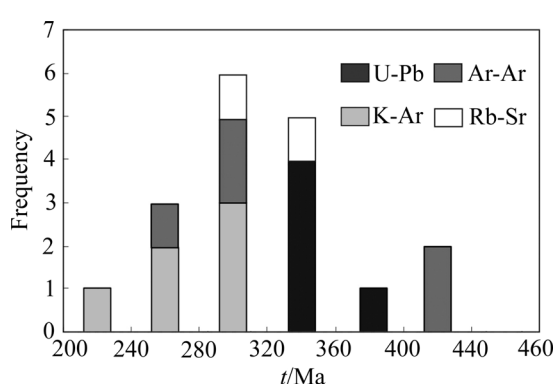


图6 滩间山金矿区同位素年代图

Fig. 6 Data of isotopic age from Tanjianshan gold deposit

形成万洞沟群的含 Au(13.5×10^{-9} ~ 32.0×10^{-9}) 黑色岩层^[37], 该岩层为金成矿物质的主要来源。

第二阶段: 海西早期构造挤压 Au 矿化富集阶段(见图 7(b))。随着柴达木陆块与祁连陆块的陆陆碰撞^[35],

矿区内万洞沟群在动力变质和热变质作用下形成韧性剪切带^[36, 55], 同时少量基性、中酸性岩体侵入^[56], 万洞沟群地层中的 Au 开始迁移并富集成矿, 即灰黑色含炭千枚岩中浸染状黄铁矿 Py1 形成于该时期。

第三阶段: 海西晚期构造伸展阶段 Au 矿化叠加富集阶段(见图 7(c))。随着碰撞造山进入后期, 挤压环境向伸展构造阶段转变, 形成了区内较大规模的碰撞后斜长花岗斑岩^[44], 花岗岩斑岩^[57]及少量岩脉^[58], 这些岩体、岩脉代表了在同一造山过程中岩浆不同阶段演化和成矿事件, 即灰黑色含炭千枚岩石英内浸染状与块状黄铁矿 Py2、Py3 形成于该时期。

第四阶段: 印支期柴北缘-祁连地体地壳抬升 Au 矿化再富集阶段(见图 7(d))。随着陆内造山运动开始, 矿区内构造再次活化, 形成了闪长玢岩和云煌岩等侵入体, 带来了大量的含金流体^[27-28], 其他含矿岩体的全岩 Rb-Sr、K-Ar、Ar-Ar 等同位素年代数据 330~209 Ma 也记录了这一时期多次的构造热事件^[27-28, 59-60],

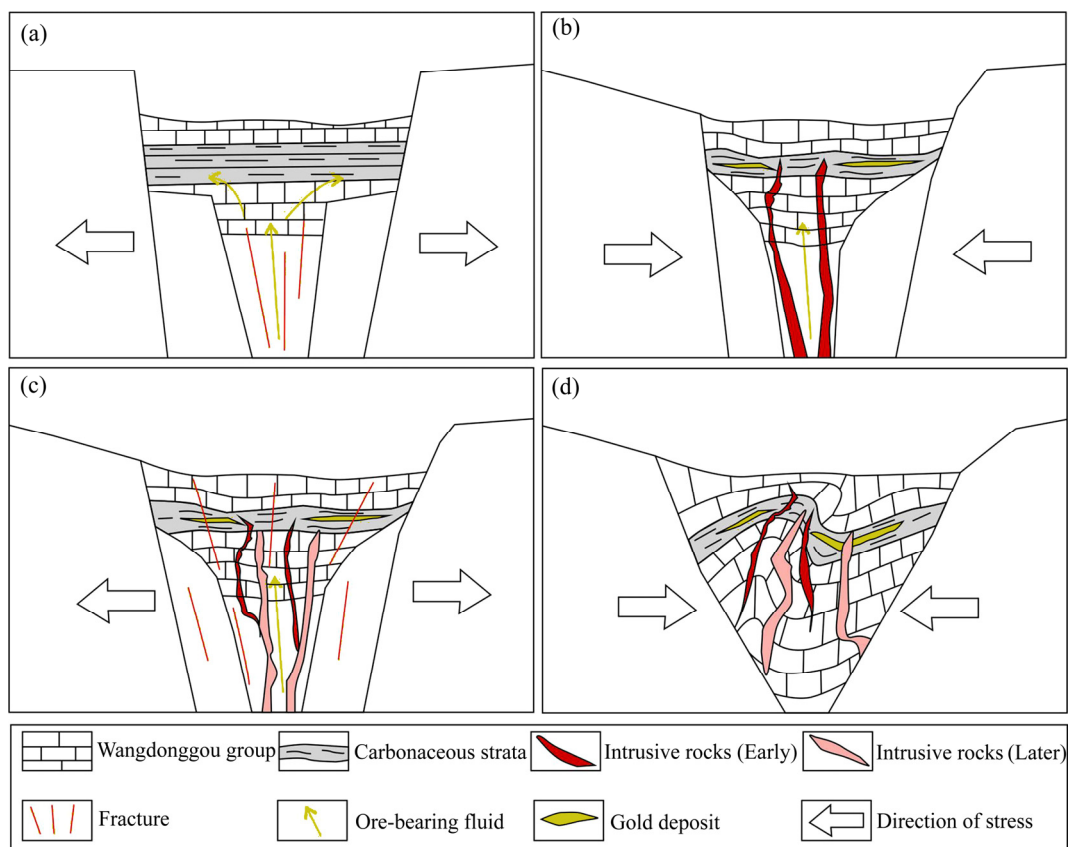


图7 滩间山金矿成矿演化过程(底图据文献[61]): (a) 中元古界裂谷期–Au 初步富集阶段; (b) 海西早期构造挤压–Au 矿化富集阶段;

Fig. 7 Sketchshowing the evolution of mineralization in Tanjianshan gold deposit (Derived from Ref. [61]): (a) Rift stage during Meso-proterozoic-Au preliminary enrichment stage; (b) Structural extrusion during early Hercynian-Au enrichment stage; (c) Tectonic stretching during late Hercynian-Au re-enrichment stage; (d) Crustal uplift of Northern Qaidam-Qilian block during Indosinian-Au re-enrichment stage

含矿流体进一步提取了矿源层中的 Au 元素，并将这些元素带到前期已形成矿化的部位，发生了金的叠加富集，形成了有价值的工业矿体，蚀变花岗斑岩脉岩中 Py4 即形成于该时期。

6 结论

1) 滩间山金矿区内的黄铁矿的 Co 和 Ni 含量指示了金矿成因来自沉积改造和岩浆作用。滩间山金矿区内的四种类型黄铁矿，从 Py1、Py2、Py3 到 Py4，Co/Ni 比值逐渐升高，表现出黄铁矿形成温度由低温到高温，其微量元素的相关性也指示其经历了多期成矿热事件。

2) 滩间山金矿床中不同类型的黄铁矿是海西早期和海西晚期–印支复合造山过程的产物，其成矿经

历了至少四个阶段，其中黄铁矿分布对应了海西早期构造挤压 Au 矿化富集阶段(Py1)、海西晚期构造伸展阶段 Au 矿化叠加富集阶段(Py2 和 Py3)、印支期柴北缘–祁连地体地壳抬升 Au 矿化再富集阶段(Py4)。

致谢

感谢审稿老师和编辑老师给本文提出的宝贵意见，在此表示衷心感谢。

REFERENCES

- [1] LARGE R R, DANYUSHEVSKY L, HOLLIT C, MASLENNIKOV V, MEFFRE S, GILBERT S, BULL S, SCOTT R, EMSBO P, THOMAS H, SINGH B, FOSTER J. Gold and trace element zonation in pyrite using a laser imaging technique: Implications for the timing of gold in

- ogenetic and carlin-style sediment-hosted deposits[J]. *Economic Geology*, 2009, 104(5): 635–668.
- [2] LIU An-lu, ZHANG Xiao-jun, THOMAS U, ZHANG J, JIANG Man-rong, LIU Wen-hao. Geology, geochronology and fluid characteristics of the Pingqiu gold deposit, Southeastern Guizhou Province, China[J]. *Ore Geology Reviews*, 2017, 89: 187–205.
- [3] 周涛发, 张乐骏, 袁峰, 范裕, David R C. 安徽铜陵新桥 Cu-Au-S 矿床黄铁矿微量元素 LA-ICP-MS 原位测定及其对矿床成因的制约[J]. 地学前缘, 2010, 17(2): 306–319.
- ZHOU Tao-fa, ZHANG Le-jun, YUAN Feng, FAN Yu, David R C. LA-ICP-MS in situ trace element analysis of pyrite from the Xinqiao Cu-Au-S deposit in Tongling, Anhui, and its constraints on the ore genesis[J]. *Earth Science Frontiers*, 2010, 17(2): 306–319.
- [4] BRALIA A, SABATINI G, TROJA F. A revaluation of the Co/Ni ratio in pyrite as geochemical tool in ore genesis problems[J]. *Mineralium Deposita*, 1979, 14(3): 353–374.
- [5] HEINRICH C A. The physical and chemical evolution of low-salinity magmatic fluids at the porphyry to epithermal transition: A thermodynamic study[J]. *Mineralium Deposita*, 2005, 39(8): 864–889.
- [6] 陶诗龙, 赖健清, 张建东, 钱丽华, 胡理芳, 曹蓉, 游琲, 黄冲, 李廖辉, 黄锐, 梁崇高. 广西龙头山金矿载金黄铁矿地球化学特征[J]. 中国有色金属学报, 2017, 27(6): 1263–1279.
- TAO Shi-long, LAI Jian-qian, ZHANG Jian-dong, QIAN Lihua, HU Li-fang, CAO Rong, YOU Bei, HUANG Chong, LI Liao-hui, HUANG Rui, LIANG Chong-gao. Geochemical characteristics of auriferous pyrite in Longtoushan gold deposit, Guangxi Province, China[J]. *The Chinese Journal of Nonferrous Metals*, 2017, 27(6): 1263–1279.
- [7] 邵拥军, 谢友良, 冯雨周, 张宇, 刘忠法, 蒋梦同. 甘肃李坝金矿床金属硫化物成分特征及其意义[J]. 中国有色金属学报, 2017, 27(12): 2567–2582.
- SHAO Yong-jun, XIE You-liang, FENG Yu-zhou, ZHANG Yu, LIU Zhong-fa, JIANG Meng-tong. Implication and component characteristics of metal sulfides in Liba gold deposit, Gansu province[J]. *The Chinese Journal of Nonferrous Metals*, 2017, 27(12): 2567–2582.
- [8] 蔡鹏捷, 许荣科, 朱本杰, 陶长才, 廖明迅, 刘嘉, 王红军, 卢锐, 杜文洋. 湖北嘉鱼蛇屋山红土型金矿研究回顾与展望[J]. 地质论评, 2016, 62(2): 389–397.
- CAI Peng-jie, XU Rong-ke, ZHU Ben-jie, TAO Chang-cai, LIAO Ming-xun, LIU Jia, WANG Hong-jun, LU Rui, DU Wen-yang. Review and prospect of Shewushan Lateritic Gold Deposit, Jiayu, Hubei Province[J]. *Geological Review*, 2016, 62(2): 389–397.
- [9] 毕诗健, 李占轲, 唐克非, 高凯. 小秦岭东桐峪金矿床黄铁矿 LA-ICP-MS 微量元素特征及其成矿意义[J]. 地球科学, 2016, 41(7): 1121–1140.
- BI Shi-jian, LI Zhan-ke, TANG Ke-fei, GAO Kai. LA-ICP-MS in situ trace element analysis of pyrite from Dongtongyu gold deposit and its metallogenetic significance, Xiaoqinling gold district [J]. *Earth Science*, 2016, 41(7): 1121–1140.
- [10] CAREW M J, MARK G, OLIVER N H S, PEARSON N. Trace element geochemistry of magnetite and pyrite in Fe oxide (\pm Cu Au) mineralised systems: Insights into the geochemistry of ore-forming fluids[J]. *Geochimica Et Cosmochimica Acta*, 2006, 70(18): A83–A83.
- [11] COOK N J, CIOBANU C L, MAO J W. Textural control on gold distribution in As-free pyrite from the Dongping, Huangtuliang and Houguo gold deposits, North China Craton (Hebei Province, China)[J]. *Chemical Geology*, 2009, 264(1/4): 101–121.
- [12] KOGLIN N, FRIMMEL H E, MINTER W E L, BRATZ H. Trace-element characteristics of different pyrite types in Mesoarchaean to Palaeoproterozoic placer deposits[J]. *Mineralium Deposita*, 2010, 45 (3): 259–280.
- [13] NADOLL P, KOENING A E. LA-ICP-MS of magnetite: Methods and reference materials[J]. *Journal of Analytical Atomic Spectrometry*, 2011, 26(9): 1872–1877.
- [14] MORISHITA Y, SHIMADA N, SHIMADA K. Invisible gold in arsenian pyrite from the high-grade Hishikari gold deposit, Japan: Significance of variation and distribution of Au/As ratios in pyrite[J]. *Ore Geology Reviews*, 2018, 95: 79–93.
- [15] YUAN Mao-wen, LI Sheng-rong, LI Cheng-lu, SANTOSH M, ALAM M, ZENG Yong-jie. Geochemical and isotopic composition of auriferous pyrite from the Yongxin gold deposit, central Asian orogenic belt: Implication for ore genesis [J]. *Ore Geology Reviews*, 2018, 93: 255–267.
- [16] WANG Jian-ping, LIU Zheng-jiang, LIU Jia-jun, ZENG Xiang-tao, WANG Ke-xin, LIU Bi-zheng, ANG Huan, LIU Chong-hao, ZHANG Fang-fang. Trace element compositions of pyrite from the Shuangwang gold breccias, western Qinling orogen, China: Implications for deep ore prediction[J]. *Journal of Earth Science*, 2018, 29(3): 564–572.

- [17] ZHANG Yong-chao, GAO Sun-bao, ZHENG You-ye, JIANG Jun-sheng, ZHANG Shu-zhi, JIANG Xiao-jia, GUO Xin-ran. Mineralogy, fluid inclusions and C–H–O–S–Pb isotopes of the Palaeocene Longgen Pb-Zn deposit in the western Nyainqntanglha belt, Tibet [J]. *Ore Geology Reviews*, 2018, 102: 18–43.
- [18] NIE Xiao, SHEN Jun-feng, LIU Hai-ming, DU Bai-song, WANG Shu-hao, LI Jie, XU Li-wei, WANG Ran. Geochemistry of pyrite from the Gangcha Gold Deposit, West Qinling Orogen, China: Implications for ore genesis[J]. *Acta Geologica Sinica-English Edition*, 2017, 91(6): 2164–2179.
- [19] GRANT H L J, HANNINGTON M D, PETERSEN S, FRISCHE M, FUCHS S H. Constraints on the behavior of trace elements in the actively-forming TAG deposit, Mid-Atlantic Ridge, based on LA-ICP-MS analyses of pyrite[J]. *Chemical Geology*, 2018, 498: 45–71.
- [20] LIU Zhong-fa, SHAO Yong-jun, ZHOU Hao-di, LIU Nan, HUANG Kuan-xin, LIU Qing-quan, ZHANG Jian-dong, WANG Cheng. Major and trace element geochemistry of pyrite and pyrrhotite from stratiform and lamellar orebodies: Implications for the ore genesis of the Dongguashan Copper (Gold) Deposit, Eastern China[J]. *Minerals*, 2018, 8(9): 380.
- [21] WARD J, MAVROGENES J, MURRAY A, HOLDEN P. Trace element and sulfur isotopic evidence for redox changes during formation of the Wallaby Gold Deposit, Western Australia [J]. *Ore Geology Reviews*, 2017, 82: 31–48.
- [22] ZHOU Ling-li, MCKENNA C A, LONG D G F, KAMBER B S. LA-ICP-MS elemental mapping of pyrite: An application to the Palaeoproterozoic atmosphere[J]. *Precambrian Research*, 2017, 297: 33–55.
- [23] DEHNAVI A S, MCFARLANE C R M, LENTZ D R, WALKER J A. Assessment of pyrite composition by LA-ICP-MS techniques from massive sulfide deposits of the bathurst mining camp, Canada: From textural and chemical evolution to its application as a vectoring tool for the exploration of VMS deposits[J]. *Ore Geology Reviews*, 2018, 92: 656–671.
- [24] GREGORY M J, LANG J R, GILBERT S, HOAL K O. Geometallurgy of the pebble porphyry copper-gold-molybdenum deposit, Alaska: Implications for gold distribution and paragenesis[J]. *Economic Geology*, 2013, 108(3): 463–482.
- [25] 彭南海, 邵拥军, 刘忠法, 汪程. 山西义兴寨金矿田成矿机理研究: 来自同位素和流体包裹体的证据[J]. 中国有色金属学报, 2017, 27(2): 305–317.
- [26] PENG Nan-hai, SHAO Yong-jun, LIU Zhong-fa, WANG Cheng. Metallogenetic mechanism of Yixingzhai gold ore field in Fanshi county, Shanxi province: Evidences from isotopes and fluid inclusion[J]. *The Chinese Journal of Nonferrous Metals*, 2017, 27(2): 305–317.
- [27] 赖健清, 鞠培姣, 周凤. 青海省果洛龙洼金矿多因复成矿作用[J]. 中国有色金属学报, 2016, 26(2): 402–414.
- [28] LAI Jian-qing, JU Pei-jiao, ZHOU Feng. Polygenetic compound mineralization of Guoluolongwa gold deposit in Qinghai Province, China[J]. *The Chinese Journal of Nonferrous Metals*, 2016, 26(2): 402–414.
- [29] ZHANG De-quan, SHE Hong-quan, FENG Cheng-you, LI Da-xin, LI Jin-wen. Geology, age, and fluid inclusions of the Tanjianshan gold deposit, western China: Two orogenies and two gold mineralizing events[J]. *Ore Geology Reviews*, 2009, 36(1): 250–263.
- [30] 崔艳合, 张德全, 李大新, 顾光先, 丰成友. 青海滩间山金矿床地质地球化学及成因机制[J]. 矿床地质, 2000, 19(3): 211–222.
- [31] CHUI Yan-he, ZHANG De-quan, LI Da-xin, GU Guang-xian, FENG Chen-you. Geology, geochemistry and genesis of the Tanjianshan gold deposit, Qinghai province[J]. *Mineral deposit*, 2000, 19(3): 211–222.
- [32] YANG Jing-sui. Early Paleozoic north Qaidam UHP metamorphic belt on the northeastern Tibetan plateau and a paired subduction model[J]. *Terra Nova*, 2002, 14: 397–404.
- [33] SONG Shu-guang, ZHANG Li-fei, NIU Yao-lin, SU Li, SONG Biao, LIU Dunyi. Evolution from oceanic subduction to continental collision: A case study from the northern Tibetan plateau based on geochemical and geochronological data[J]. *Journal of Petrology*, 2006, 47(3): 435–455.
- [34] SONG Shu-guang, NIU Yao-lin, SU Li, ZHANG Cong, ZHANG Li-fei. Continental orogenesis from ocean subduction, continent collision/subduction, to orogen collapse, and orogen recycling: The example of the north Qaidam UHPM belt, NW China[J]. *Earth Science Reviews*, 2014, 129: 59–84.
- [35] 蔡鹏捷, 许荣科, 郑有业, 陈鑫, 刘嘉, 俞军真. 柴北缘从大洋俯冲到陆陆碰撞: 来自开屏沟造山带M型橄榄岩的证据[J]. 地球科学, 2018, 43(8): 2875–2892.
- [36] CAI Peng-jie, XU Rong-ke, ZHENG You-ye, CHEN Xin, LIU Jia, YU Jun-zhen. From oceanic subduction to continental collision in north Qaidam: Evidence from Kaipinggou orogenic M-type peridotite[J]. *Earth Science*, 2018, 43(8): 2875–2892.

- [33] 陈鑫, 郑有业, 许荣科, 蔡鹏捷, 林成贵, 白杰, 孙述海, 鲁立辉. 柴北缘鱼卡榴辉岩型金红石矿床金红石矿物学、元素地球化学及成因[J]. 岩石学报, 2018, 34(6): 1685–1703.
- CHEN Xin, ZHENG You-ye, XU Rong-ke, CAI Peng-jie, LIN Chen-gui, BAI Jie, SUN Shu-hai, LU Li-hui. Mineralogical, trace element composition of rutile and genesis of eclogite-type rutile deposit from the Yuka terrane, North Qaidam UHPM belt[J]. Acta Petrologica Sinica, 2018, 34(6): 1685–1703.
- [34] CHEN Xin, ZHENG You-ye, XU Rong-ke, CAI Peng-jie. Petrology and geochemistry of high niobium eclogite in the North Qaidam orogen, Western China: Implications for an eclogite facies metamorphosed island arc slice[J]. Journal of Asian Earth Sciences, 2018, 164: 380–397.
- [35] CHEN Xin, XU Rong-ke, SCHERTL H P, ZHENG You-ye. Eclogite-facies metamorphism in impure marble from North Qaidam orogenic belt: Geodynamic implications for early Paleozoic continental-arc collision[J]. Lithos, 2018, 310-311: 201–224.
- [36] CHEN Xin, XU Rong-ke, ZHENG You-ye, JIANG Xiao-jia, DU Wen-yang. Identifying potential Au-Pb-Ag mineralization in SE Shuangkoushan, North Qaidam, Western China: Combined log-ratio approach and singularity mapping[J]. Journal of Geochemical Exploration, 2018, 189: 109–121.
- [37] 张德全, 党兴彦, 余宏全, 李大新, 丰成友, 李进文. 柴北缘-东昆仑地区造山型金矿床的 Ar-Ar 测年及其地质意义[J]. 矿床地质, 2005, 24(2): 87–98.
- ZHANG De-quan, DANG Xing-yan, SHE Hong-quan, LI Da-xin, FENG Cheng-you, LI Jin-wen. Ar-Ar dating of orogenic gold deposits in northern margin of Qaidam and East Kunlun Mountains and its geological significance[J]. Mineral Deposits, 2005, 24(2): 87–98.
- [38] 张德全, 张慧, 丰成友, 余宏全, 李进文, 李大新. 柴北缘-东昆仑地区造山型金矿床的流体包裹体研究[J]. 中国地质, 2007, 34(5): 843–854.
- ZHANG De-quan, ZHANG Hui, FENG Cheng-you, SHE Hong-quan, LI Jin-wen, LI Da-xin. Fluid inclusions in orogenic gold deposits in the northern Qaidam margin-East Kunlun region[J]. Geology in China, 2007, 34(5): 843–854.
- [39] 许荣科, 郑有业, 周宾, 吴亮, 祝海洋, 张宇, 马超, 吕登. 柴北缘绿梁山一带与造山作用相关的铜铅锌矿床成矿规律及找矿启示[J]. 西北地质, 2012, 45(1): 192–201.
- XU Rong-ke, ZHENG You-ye, ZHOU Bin, WU Liang, ZHU Hai-yang, ZHANG Yu, MA Chao, LÜ Deng. The metallogenetic regularity and inspiration prospecting of copper lead-zinc deposit associated with orogenic in the Luliangshan area northern margin of Qaidam basin[J]. Northwestern Geology, 2012, 45(1): 192–201.
- [40] 蔡鹏捷, 国显正, 郑有业, 孙述海, 刘嘉, 陈鑫, 俞军真, 许荣科. 岩浆型 Ni-Cu-PGE 硫化物矿床研究现状及进展[J]. 地质论评, 2018, 64(4): 956–979.
- CAI Peng-jie, GUO Xian-zheng, ZHENG You-ye, SU Shu-hai, LIU Jia, CHEN Xin, YU Jun-zhen, XU Rong-ke. The research situation and progress in magmatic Ni-Cu-PGE sulfide deposits[J]. Geological Review, 2018, 64(4): 956–979.
- [41] 蔡鹏捷, 许荣科, 郑有业, 范贤斌, 马超, 白杰, 陈鑫, 俞军真. 基于成矿流体包裹体的勘探—以柴北缘鱼卡造山型金矿为例[J]. 地质找矿论丛, 2018, 33(4): 651–660.
- CAI Peng-jie, XU Rong-ke, ZHENG You-ye, FAN Xian-bin, MA Chao, BAI Jie, CHEN Xin, YU Jun-zhen. Exploration guided by study on ore-forming fluid inclusions—A case study of Yuka orogenic gold deposit in north margin of Qaidam basin[J]. Contributions to Geology and Mineral Resources Research, 2018, 33(4): 651–660.
- [42] 蔡鹏捷, 张宇, 许荣科, 郑有业, 国显正, 陈鑫. 柴北缘双口山石英正长岩锆石 U-Pb 定年、地球化学及 Sr-Nd 同位素特征[J]. 大地构造与成矿学, 2019, 43(02): 322–338.
- CAI Peng-jie, ZHANG Yu, XU Rong-ke, ZHENG You-ye, GUO Xian-zheng, CHEN Xin. Zircon U-Pb geochronology, geochemistry, and Sr-Nd isotope of Shuangkoushan Quartz-syenite, Northern Qaidam, China[J]. Geotectonica et Metallogenesis, 2019, 43(02): 322–338.
- [43] 蔡鹏捷, 郑有业, 陈鑫, 白杰, 许荣科. 柴达木盆地北缘开屏沟纯橄岩中铬铁矿环带成因及其构造意义[J]. 地质学报, 2019, 93(03): 647–660.
- CAI Peng-jie, ZHENG You-ye, CHEN Xin, BAI Jie, XU Rong-ke. Genesis of the zonal texture of chromite from the Kaipigou peridotite in the northern margin of Qaidam basin and its tectonic significance[J]. Acta Geologica Sinica, 2019, 93(03): 647–660.
- [44] 贾群子, 杜玉良, 赵子基, 宋忠宝, 全守村, 陈博, 孔会磊, 栗亚芝, 李金超, 陈向阳, 张雨莲. 柴达木盆地北缘滩间山金矿区斜长花岗斑岩锆石 LA-MC-ICPMS 测年及其岩石地球化学特征[J]. 地质科技情报, 2013, 32(1): 87–93.
- JIA Qun-zi, DU Yu-liang, ZHAO Zi-ji, SONG Zhong-bao, QUAN Shou-cun, CHEN Bo, KONG Hui-lei, LI Ya-zhi, LI Jin-chao, CHEN Xiang-yang, ZHANG Yu-lian. Zircon

- LA-MC-ICPMS U-Pb dating and geochemical characteristics of the plagiogranite porphyry from Tanjianshan gold ore district in north margin of Qaidam Basin[J]. Geological Science and Technology Information, 2013, 32(1): 87–93.
- [45] ZONG Ke-qing, KLEMD R, YUAN Yu, HE Zhen-yu, GUO Jing-liang, SHI Xiao-li, LIU Yong-sheng, HU Zhao-chu, ZHANG Ze-ming. The assembly of Rodinia: The correlation of early Neoproterozoic (ca. 900 Ma) high-grade metamorphism and continental arc formation in the southern Beishan Orogen, southern Central Asian Orogenic Belt (CAOB)[J]. Precambrian Research, 2017, 290: 32–48.
- [46] HU Zhao-chu, ZHANG Wen, LIU Yong-sheng, GAO Shan, LI Ming, ZONG Ke-qing, CHEN Hai-hong, HU Sheng-hong. “Wave” signal smoothing and mercury removing device for laser ablation quadrupole and multiple collector ICP-MS analysis: Application to lead isotope analysis[J]. Analytical Chemistry, 2015, 87: 1152–1157.
- [47] LIU Yong-sheng, HU Zhao-chu, GAO Shan, GÜNTHER D, XU Juan, GAO Chang-gui, CHEN Hai-hong. In situ analysis of major and trace elements of anhydrous minerals by LA-ICP-MS without applying an internal standard[J]. Chemical Geology, 2008, 257: 34–43.
- [48] 盛继福, 李岩, 范书义. 大兴安岭中段铜多金属矿床矿物微量元素研究[J]. 矿床地质, 1999, 18(2): 153–160.
SHENG Ji-fu, LI Yan, FAN Shu-yi. A study on minor elements in minerals from polymetallic deposits in the central part of the Da Hinggan Mountains[J]. Mineral Deposits, 1999, 18(2): 153–160.
- [49] 毛先成, 潘敏, 刘占坤, 汪凡云, 邓浩, 韩建民, 樊红喜, 夏芳, 肖飞, 魏清峰, 三金柱. 西天山阿希金矿床黄铁矿微量元素 LA-ICP-MS 原位测试及其指示意义[J]. 中南大学学报(自然科学版), 2018, 49(5): 1148–1159.
MAO Xian-cheng, PAN Min, LIU Zhan-kun, WANG Fan-yun, DENG Hao, HAN Jian-min, FAN Hong-xi, XIA Fang, XIAO Fei, WEI Qing-feng, SAN Jin-zhu. LA-ICP-MS trace element analysis of pyrite from Axi gold deposit in western Tianshan and its significance[J]. Journal of Central South University (Science and Technology), 2018, 49(5): 1148–1159.
- [50] 毕献武, 胡瑞忠, 彭建堂, 吴开兴. 黄铁矿微量元素地球化学特征及其对成矿流体性质的指示[J]. 矿物岩石地球化学通报, 2004, 23(1): 1–4.
BI Xian-wu, HU Rui-zhong, PENG Jian-tang, WU Kai-xin. REE and HFSE geochemical characteristics of pyrites in Yao'an Gold Deposit: Tracing ore forming fluid signatures[J]. Bulletin of Mineralogy, Petrology and Geochemistry, 2004, 23(1): 1–4.
- [51] BAJWAH Z U, SECCOMBE P K, OFFLER R. Trace element distribution, Co:Ni ratios and genesis of the Big Cadia iron-copper deposit, New South Wales, Australia[J]. Mineral Deposita, 1987, 22(4): 292–300.
- [52] 丰成友, 张德全, 李大新, 崔艳合. 青海赛坝沟金矿地质特征及成矿时代[J]. 矿床地质, 2002, 21(1): 45–52.
FENG Cheng-you, ZHANG De-quan, LI Da-xin, CUI Yan-he. Geological characteristics and ore-forming age of Saibagou Gold Deposit, Qinghai Province[J]. Mineral Deposits, 2002, 21(1): 45–52.
- [53] 寇林林, 罗明非, 钟康惠, 赵昌新. 青海五龙沟金矿矿区 I 号韧性剪切带~(40)Ar/~(39)Ar 年龄及地质意义[J]. 新疆地质, 2010, 28(3): 330–333.
KOU Lin-lin, LUO Ming-fei, ZHONG Kang-hui, ZHAO Chang-xin. 40Ar/39Ar dating of the I gold-bearing shear zone on the gold-ore collected belt of the Wulonggou, Qinghai, and its significance[J]. Xingjiang geology, 2010, 28(3): 330–333.
- [54] 李金超, 孔会磊, 栗亚芝, 南卡俄吾, 贾群子, 国显正, 张斌. 青海东昆仑瑙木浑金矿蚀变绢云母 Ar-Ar 年龄、石英闪长岩锆石 U-Pb 年龄和岩石地球化学特征[J]. 地质学报, 2017, 91(5): 979–991.
LI Jing-chao, KONG Hui-lei, LI Ya-zhi, Namkha N, JIA Qun-zi, GUO Xian-zheng, ZHANG Bin. Ar-Ar age of altered sericite, zircon U-Pb age of quartz diorite and geochemistry of the Naomuhun Gold Deposit, East Kunlun[J]. Acta Geological Sinica, 2017, 91(5): 979–991.
- [55] 张德全, 丰成友, 李大新, 徐文艺, 阎升好, 余宏全, 董英君, 崔艳合. 柴北缘-东昆仑地区的造山型金矿床[J]. 矿床地质, 2001, 20(2): 137–146.
ZHANG De-quan, FENG Cheng-you, LI Da-xin, XU Wen-ji, YAN Sheng-hao, SHE Hong-quan, DONG Ying-jun, CUI Yan-he. Orogenic gold deposits in the North Qaidam and East Kunlun orogen, West China [J]. Mineral Deposits, 2001, 20(2): 137–146.
- [56] 李世金. 祁连造山带地球动力学演化与内生金属矿产成矿作用研究[D]. 长春: 吉林大学, 2011: 1–204.
LI Shi-jin. Geodynamic evolution of Qilian orogenic belt and metallogenesis of endogenous metals[D]. Changchun: Jinlin University, 2011: 1–204.
- [57] 张延军. 青海省滩间山地区内生金属矿产成矿作用研究[D]. 长春: 吉林大学, 2017: 1–182.

- Study on the Metallogenesis of endogenous metallic deposits in Tanjianshan area in Qinghai Province[D]. Changchun: Jinlin University, 2017: 1–182.
- [58] 张博文. 青海南祁连造山带内生金属矿床成矿作用研究[D]. 长春: 吉林大学, 2010: 1–192.
ZHANG Bo-wen. Study on metalliferous deposits mineralization in Southern Qilian Orogenic Belt, Qinghai Province[D]. Changchun: Jinlin University, 2010: 1–192.
- [59] 国家辉. 滩间山金矿田岩浆岩特征及其与金矿化关系[J]. 贵金属地质, 1998, 7(2): 96–103.
GUO Jia-hui. Characteristics of magmatite and its relation to gold mineralization of Tanjianshan gold field[J]. Journal of Precious Metallic Geology, 1998, 7(2): 96–103.
- [60] 林文山, 范照雄, 贺领兄. 青海省大柴旦青龙沟金矿床地质特征、找矿标志和找矿方向[J]. 矿产与地质, 2006, 20(2): 122–127.
LIN Wen-shan, FAN Zhao-xiong, HE Ling-xiong. Geological characteristics, ore indicators and orientation of Qinglonggou gold deposit, Dachaidan, Qinghai[J]. Mineral Resources and Geology, 2006, 20(2): 122–127.
- [61] 王旭阳, 王旭阳, 王宏阳, 王方里. 青海滩间山金矿成矿构造机制研究[J]. 地质学刊, 2015, 39(2): 225–230.
WANG Xu-yang, WANG Xu-yang, WANG Hong-yang, WANG Fang-li. Metallogenic tectonic mechanism of the Tanjianshan gold deposit in Qinghai Province[J]. Journal of Geology, 2015, 39(2): 225–230.

Trace elements characteristics of pyrites in Tanjianshan gold deposit, Northern Qaidam, China: Implications for multiple gold mineralizing events

CAI Peng-jie^{1,2}, ZHENG You-ye^{2,3}, LU Li-hui³, CHEN Xin³, YIN Yue-ming³, HOU Wei-dong³, HANG Deng-hui³, XU Rong-ke²

(1. Guangzhou Marine Geological Survey, China Geological Survey, Guangzhou, 510760, China;
2. Institute of Geological Survey, China University of Geosciences, Wuhan 430074, China;
3. The Faculty of Earth Resources, China University of Geosciences, Wuhan 430074, China)

Abstract: The Tanjianshan gold deposit, locates in the northern Qaidam metallogenic belt, is a typical orogenic gold deposit. Laser-ablation inductively coupled plasma mass spectrometry (LA-ICP-MS) analysis was conducted to determine the chemical composition of the bearing-gold pyrites in the Tanjianshan gold deposit. Four types of pyrites were recognized through detailed field work and microscopic studies. The first type of pyrites (Py1) is mainly present in altered carbonaceous mylonite schist. The second type of pyrites (Py2) occurs as veins or veinlets in the quartz. And the third type of pyrites (Py3) appears as mass in the quartz. The fourth type of pyrites (Py4) is mainly present in the vein rock, which is intruded into the mylonite schist. The results show that these pyrites indicate that the temperatures at which they formed increases from Py1 to Py4. According to the epochal characteristics of the Tanjianshan gold deposit, the four types of pyrites correspond to the later three stages in the metallogenic evolution of Tanjianshan gold deposit: Py1 was formed in tectonic extrusion environment during early Hercynian, Au began to enrich at the stage; Py2 and Py3 were produced in tectonic extension environment during later Hercynian, which Au occurs superposition; Py4 was generated in crustal uplift of the Qaidam and Qilian block, Au occurs enrichment again.

Key words: Tanjianshan; orogenic gold deposit; pyrite; trace elements; metallogenic evolution

Foundation item: Project(IRT14R54) supported by the Program for Cheung Kong Scholars and Innovative Research Team of Ministry of Education, China; Project(21201011000150004, DD20190069) supported by the Program for China Geological Survey

Received date: 2018-08-26; **Accepted date:** 2019-01-21

Corresponding author: XU Rong-ke; Tel: +86-18971071732; E-mail: xurongke1968@126.com

(编辑 何学锋)